Journal of the Korean Physical Society, Vol. 70, No. 1, January 2017, pp. 85∼88

Crystallograhic and Magnetic Properties of $Fe_{1-x}Ni_xGa_2O_4$

Bo Ra Myoung, Jung Tae Lim and Chul Sung Kim*
Department of Physics, Kookmin University, Seoul 02707, Korea

(Received 30 November 2016, in final form 9 December 2016)

We report the crystallographic and magnetic effects on inverse spinel $Fe_{1-x}Ni_xGa_2O_4$ ($0.0 \leq x \leq 0.9$) due to doped Ni cations. The crystalline structures of $Fe_{1-x}Ni_xGa_2O_4$ ($0.0 \leq x \leq 0.9$) were examined by using a Philips X'Pert diffractometer with a Cu $K\alpha$ radiation ($\lambda = 1.5406$ Å) source and analyzed with the Rietveld refinement method. The crystal structures were found to be inverse spinel with space group *Fd-3m*. From the Rietveld analysis, with increasing Ni concentration, the ratio of magnetic Fe^{2+} cations, compared to the total number of Fe^{2+} cations on A-site (tetrahedron) decreased from 43 to 7%, and that on B-site (octahedron) increased from 57 to 93%. The lattice constants a_0, and bond length $d_{Ga^{3+}-Fe^{2+}[Ni^{2+}]}$ on A-site and B-site decreased linearly with increasing Ni concentration. From the temperature dependence of susceptibility χ in zero-field-cooled and field-cooled magnetization under 400 Oe, with increasing Ni concentration, the sample showed a decrease in the freezing temperature T_f. Mössbauer spectra of all samples at room temperature showed 2-sets (A-site, and B-site) with large electric quadrupole splitting. The Mössbauer absorption area ratio of A-site decreased, while that of B-site increased with increasing Ni concentration, which is accord with the Rietveld refinement analysis of the XRD results.

PACS numbers: 61.10.Nz, 76.80.+y, 75.60.Ej, 75.10.Nr
Keywords: $Fe_{1-x}Ni_xGa_2O_4$, Mössbauer spectroscopy, Freezing temperature
DOI: 10.3938/jkps.70.85

I. INTRODUCTION

Recently, AGa_2S_4 (A = Mn, Ni, Fe, Co, Zn), Me_4B (B = P, As), Fe_2OBO_3, and AB_2O_4 materials have been investigated because of their quantum mechanical characteristics, such as its exhibiting spin-frustration, its being a spin-glass, its having incommensurate short-range order, and its being a quantum spin liquid due to spin-disorder at low temperatures [1–11]. Especially, the antiferromagnetic material $FeGa_2O_4$, which is a spin-glass system, has been used for its freezing behavior at low temperatures [12–14]. $FeGa_2O_4$ has exhibited a superparamagnetic effect, atomic short-range-order, and incommensurate spin structure, despite the strong antiferromagnetic bonds at low temperatures. Again, interestingly, $FeGa_2O_4$ has been reported to be inverse cubic spinel $[Fe_{0.05}Ga_{0.95}][Fe_{0.95}Ga_{1.05}]O_4$, in which Fe^{3+} occupies on A-site (tetrahedron) and Fe^{2+} occupies on B-site (octahedron) [15,16]. However, $FeGa_2O_4$ has also been observed to be inverse spinel that has A, and B sites with Fe^{2+} cations of $FeGa_2O_4$ [14]. Therefore, an investigation of crystallographic structure from quantum-mechanical aspects is important.

In this paper, we present effects of Ni-cations doping on the crystallographic properties on $Fe_{1-x}Ni_xGa_2O_4$ ($0.0 \leq x \leq 0.9$) by using a Rietveld refinement of the X-ray diffraction patterns and a Mössbauer analysis at room temperature. Also, in this research, we investigated the magnetic properties to find evidence for spin-glass behaviors at low temperature from superconducting quantum interference device (SQUID) magnetometer.

II. EXPERIMENTS

The polycrystalline samples of $FeGa_2O_4$ doped with Ni-cations were synthesized by using a standard solid-state reaction method. Mixed powders of Fe (99.99%), Fe_2O_3 (99.995%), Ni_2O_3 (99.995%), and Ga_2O_3 (99.99%) were ground and pressed into pellets. After these samples had been annealed at 1000 °C (x = 0.0), 1050 °C (x = 0.1, 0.3), and 1100 °C (x = 0.5, 0.7, 0.9) for 2 days, they were slowly cooled to room temperature in evacuated quartz ampoules with nitrogen gas for 6 days. The crystalline structures of samples were examined by using a Philips X'Pert diffractometer with Cu $K\alpha$ radiation ($\lambda = 1.5406$ Å) source and an analysis with a Rietveld refinement. The magnetic property for spin-freezing was measured with a superconducting quantum-interference device (SQUID) magnetometer. The Mössbauer spectra were recorded using a conventional spectrometer of the electromechanical type with a ^{57}Co source in a rhodium matrix.

*E-mail: cskim@kookmin.ac.kr; Fax: +82-2-910-5170

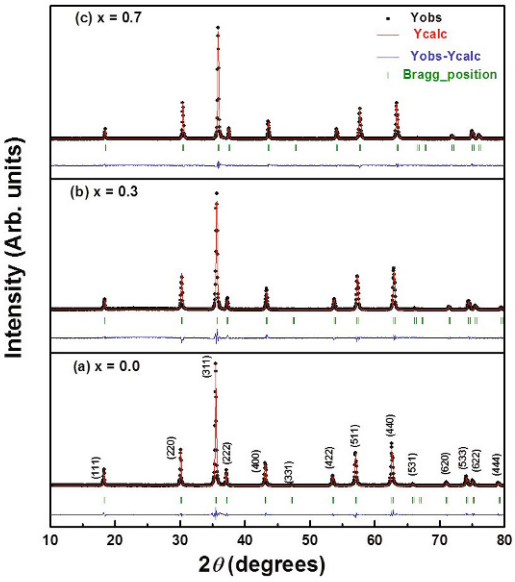

Fig. 1. (Color online) Refined x-ray diffraction patterns of $Fe_{1-x}Ni_xGa_2O_4$ at room temperature for (a) $x = 0.0$, (b) $x = 0.3$, and (c) $x = 0.7$, respectively. The solid circles represent the observed pattern; continuous lines represent the calculated and difference obs-cal patterns. The tick markers correspond to the positions of the allowed Bragg reflections.

III. RESULTS AND DISCUSSION

The crystal structures of $Fe_{1-x}Ni_xGa_2O_4$ ($0.0 \leq x \leq 0.9$) were determined by using Rietveld refinement. From the Rietveld refinement of the room temperature X-ray diffraction patterns of $Fe_{1-x}Ni_xGa_2O_4$, the Bragg factors RB and the structure factors RF were less than 4%. Figure 1 shows the X-ray diffraction patterns of $Fe_{1-x}Ni_xGa_2O_4$ (0.0, 0.3, and 0.7) polycrystalline samples at room temperature. From the analysis of the X-ray diffraction patterns, the crystal structures was found to be inverse spinel with the formula $[(Fe^{2+}, Ni^{2+})_{1-y}Ga_y^{3+}]_A[(Fe^{2+}, Ni^{2+})_yGa_{2-y}^{3+}]_BO_4^{2-}$ and space group *Fd-3m*, as in Ref. 14.

Table 1 show that the lattice constants and ratio for each element on A and B sites for $Fe_{1-x}Ni_xGa_2O_4$ ($0.0 \leq x \leq 0.9$). With increasing Ni concentration, the ratio of magnetic Fe^{2+} cations on A-site (tetrahedron) decreases from 43 to 7%, and that of B-site (octahedron) increases from 57 to 93% at a constant rate. Also, substitution of Ni in $FeGa_2O_4$ is attributed to Ga^{3+} occupying of the tetrahedral sites. Moreover, the lattice constant a_0, and bond length $d_{Ga^{3+}-Fe^{2+}[Ni^{2+}]}$ on B-site were observed to decrease linearly with increasing Ni concentration, as shown in Fig. 2. This is due to the ionic radius of Fe^{2+} (0.77 Å) being larger than that of Ni^{2+} (0.72 Å), which is consistent with Vegard's law [17].

Magnetization curves for $Fe_{1-x}Ni_xGa_2O_4$ were measured at temperatures from 4.2 to 300 K, and the results

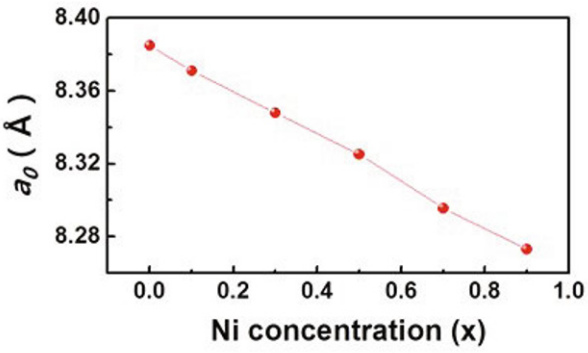

Fig. 2. (Color online) Lattice constant a_0 of $Fe_{1-x}Ni_xGa_2O_4$ as a function of the Ni concentration at room temperature [RT].

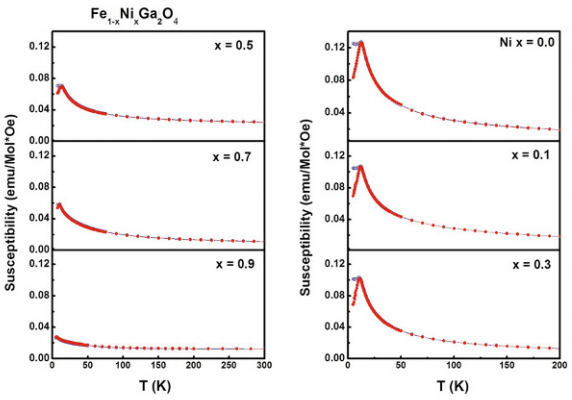

Fig. 3. (Color online) Temperature dependence of the susceptibility χ in zero-field-cooled (ZFC) and field-cooled (FC) magnetization under 400 Oe for $Fe_{1-x}Ni_xGa_2O_4$ ($x = 0.0$, 0.1, 0.3, 0.5, 0.7, and 0.9). Solid symbols are the ZFC data, and open symbols are the FC data.

are shown in Fig. 3, which presents the temperature dependence of susceptibility χ in zero-field-cooled (ZFC) and field-cooled (FC) magnetization under 400 Oe. The solid symbols are the ZFC data, and the open symbols are the FC data. All samples were observed to have a cusp in the ZFC measurement due to the spin-freezing behavior in the spin glass system at low temperatures [12,14]. Also, the magnetic irreversibility appears at the freezing temperature as a spin-freezing transition due to the thermodynamic transition in the spin glass system. The sample shows a decrease in the freezing temperature T_f of $Fe_{1-x}Ni_xGa_2O_4$ to 12.42, 12.04, 10.8, 8.9, 6.99, and 6.2 K for $x = 0.0$, 0.1, 0.3 0.5, 0.7, and 0.9 respectively, with increasing Ni concentration, as shown in Fig. 4. This can be explained by the antiferromagnetic ordering being depressed gradually due to the spin-freezing and spin-spin interaction as changes from an antiferromagnetic to a paramagnetic behavior with increasing x for

Table 1. The XRD refinement parameters of $Fe_{1-x}Ni_xGa_2O_4$ at room temperature for a *Fd-3m* inverse spinel; the lattice constants and ratios for each of elements on A and B-sites.

x(Ni)	a_0 (Å)	b_0 (Å)	c_0 (Å)	Fe^{+2}(A)	Fe^{+2}(B)	Ni^{+2}(A)	Ni^{+2}(B)	Ga^{+3}(A)	Ga^{+3}(B)	Vol.(Å^3)
0	8.385	8.385	8.385	0.430	0.570	0.000	0.000	0.570	1.430	589.476
0.1	8.370	8.370	8.370	0.378	0.521	0.039	0.061	0.582	1.418	586.315
0.3	8.348	8.348	8.348	0.261	0.439	0.112	0.188	0.627	1.373	581.759
0.5	8.325	8.325	8.325	0.178	0.322	0.174	0.326	0.648	1.352	577.037
0.7	8.296	8.296	8.296	0.084	0.216	0.197	0.503	0.719	1.281	570.905
0.9	8.273	8.273	8.273	0.007	0.093	0.215	0.685	0.778	1.222	565.247
	(±0.001)	(±0.001)	(±0.001)	(±0.001)	(±0.001)	(±0.001)	(±0.001)	(±0.001)	(±0.001)	(±0.001)

Table 2. Electric quadrupole splitting ΔE_Q, isomer shift δ, and the ratio for Mössbauer absorption area ratio of A and B-site with Fe^{2+} state.

	A-site			B-site		
x(Ni)	ΔE_Q (mm/s)	δ (mm/s)	Ratio (%)	ΔE_Q (mm/s)	δ (mm/s)	Ratio (%)
0	2.683	0.929	43.12	2.683	0.929	56.88
0.3	2.910	0.959	37.26	2.910	0.959	62.74
0.5	3.130	0.956	35.58	3.130	0.956	64.42
0.7	3.259	0.937	28.15	3.259	0.937	71.85
	(±0.001)	(±0.001)	(±0.01)	(±0.001)	(±0.001)	(±0.01)

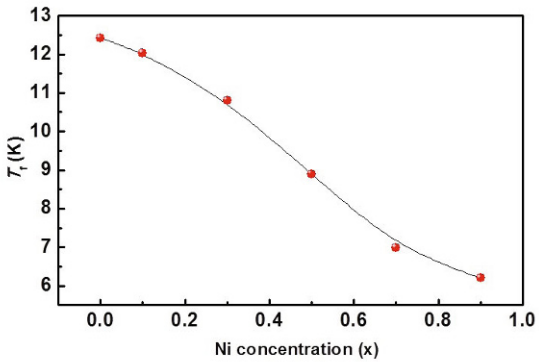

Fig. 4. (Color online) Ni substitution dependence of the freezing temperature T_f.

$Fe_{1-x}Ni_xGa_2O_4$ [5,18].

By using a least-squares fitting computer program to analyze the Mössbauer spectra at room temperature, we observed that the samples have 2-sets [A-site; tetrahedron, and B-site; octahedron] with large electric quadrupole splitting for $Fe_{1-x}Ni_xGa_2O_4$ ($0.0 \leq x \leq 0.7$), as shown in Fig. 5. From the Mössbauer absorption area ratio of A and B-sites with Fe^{2+} state, the ratio of magnetic Fe^{2+} cations on A-site, and that of B-site to the total number of Fe^{2+} ions for $Fe_{1-x}Ni_xGa_2O_4$ ($0.0 \leq x \leq 0.7$) are consistent with the results from the Rietveld refinement of the XRD data. Therefore, all samples have inverse spinel structure with the formula $[(Fe^{2+}, Ni^{2+})_{1-y}Ga^{3+}_y]_A[(Fe^{2+}, Ni^{2+})_yGa^{3+}_{2-y}]_BO^{2-}_4$. We

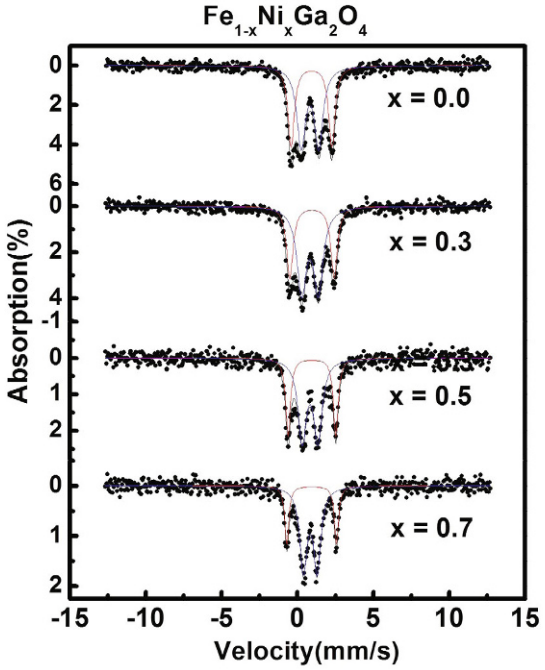

Fig. 5. (Color online) Mössbauer spectra of $Fe_{1-x}Ni_xGa_2O_4$ (x = 0.0, 0.3, 0.5, and 0.7) at room temperature [RT].

did not perform Mössbauer spectroscopy measurements on the sample with $x = 0.9$, as a slight substitution of Fe.

The values of isomer shifts (δ) at RT for A, and B

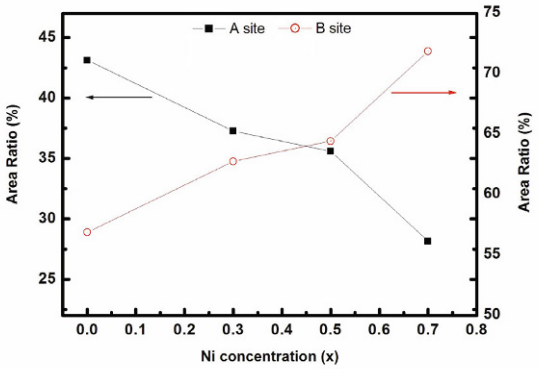

Fig. 6. (Color online) Ni substitution dependence of Mössbauer absorption area ratio at A-sites and B-sites.

sites are found to range from 0.929 to 0.937 mm/s and from 0.824 to 0.848 relative to the iron metal, which is consistent with the Fe^{2+} state, as accordance with Ref. 14. Mössbauer spectra of all samples at RT show that the Mössbauer absorption area ratio of A-site decreases from 43 to 28%, while that of B-site increases from 57 to 72% with increasing Ni concentration in accord with migration of Fe^{2+} in the A and B-sites found in the Rietveld refinement analysis (Fig. 6).

Figure 7 show the electric quadrupole splitting $\Delta E_Q = (1/2)e^2qQ[1+(1/3)\eta^2]^{1/2}$ of $Fe_{1-x}Ni_xGa_2O_4$ ($0.0 \leq x \leq 0.7$) at RT. The ΔE_Q values on A-site at RT are found to increase from 2.675 to 3.259 mm/s due to the enhanced large electrical ordering between Fe^{2+} and Fe^{2+} due to the decreasing volume of the tetrahedral structure with increasing Ni concentration. On the other hand, at B-site, they are found to decrease from 1.143 to 0.937 mm/s due to the depressed electrical ordering between Fe^{2+} and Ni^{2+} with increasing Ni concentration.

IV. CONCLUSION

In summary, the crystal structure of $Fe_{1-x}Ni_xGa_2O_4$ is found to be inverse spinel with the formula $[(Fe^{2+}, Ni^{2+})_{1-y}Ga^{3+}_y]_A[(Fe^{2+}, Ni^{2+})_yGa^{3+}_{2-y}]_BO^{2-}_4$ and space group *Fd-3m*. The lattice constants a_0 decrease linearly with increasing Ni concentration because the ionic radius of Ni^{2+} is smaller than that of Fe^{2+}. From the magnetization curves for, $Fe_{1-x}Ni_xGa_2O_4$, the sample shows a decrease in the freezing temperature T_f and changes from antiferromagnetic to paramagnetic behavior with increasing Ni concentration. The charge states of Fe ions were ferrous (Fe^{2+}), as determined from the isomer shift values at RT for the A and B-sites. The Mössbauer absorption area ratio of A-site decreases while that of B-site increases with increasing Ni concentration, which is in accord with Rietveld refinement analysis of the XRD results.

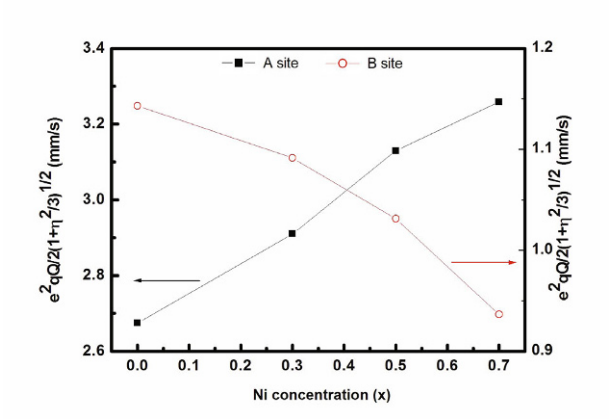

Fig. 7. (Color online) Ni substitution dependence of the electric quadrupole splitting $\Delta E_Q = (1/2)e^2qQ[1+(1/3)\eta^2]^{1/2}$ at A-sites and B-sites.

ACKNOWLEDGMENTS

This work was supported by the Mid-career Researcher Program, through the National Research Foundation of Korea (NRF), with a grant funded by the Ministry of Education, Science and Technology (MEST) (NRF-2014R1A2A1A05002488).

REFERENCES

[1] S. Nakatsuji *et al.*, Science **309**, 1697 (2005).
[2] S. Nakatsuji *et al.*, J. Phys. Condens. Matter **19**, 145232(2007).
[3] V. Tsurkan *et al.*, Phys. Rev. B **73**, 224442 (2006).
[4] N. Büttgen, A. Zymara, C. Kegler, V. Tsurkan and A. Loidl, Phys. Rev. B **73**, 132409 (2006).
[5] M. Hagiwara, N. Narita and I. Yamada, Phys. Rev. B **55**, 5615 (1997).
[6] R. Fichtl *et al.*, Phys. Rev. Lett. **94**, 027601 (2005).
[7] A. Krimmel *et al.*, Phys. Rev. B **73**, 014413 (2006).
[8] C. A. M. Mulder, A. J. Duyneveldt and J. A. Mydosh, Phys. Rev. B **23**, 1384 (1981).
[9] S. Hagemann *et al.*, Phys. Rev. Lett. **86**, 894 (2001).
[10] S. Süllow, G. J. Nieuwenhuys. A. A. Menovsky and J. A. Mydosh, Phys. Rev. Lett. **78**, 354 (1997).
[11] J. M. De Teresa *et al.*, Phys. Rev. Lett. **76**, 3392 (1996).
[12] B. R. Myoung, S. K. Han, S. J. Kim and C. S. Kim, IEEE Trans. Magn. **48**, 1567 (2012).
[13] C. A. M. Mulder, A. J. Duyneveldt and J. A. Mydosh, Phys. Rev. B **23**, 1384 (1981).
[14] J. Ghose, G. C. Hallam and D. A. Read, J. Phys. C: Solid State Phys. **10**, 1051 (1977).
[15] S. Laurent *et al.*, Chem. **108**, 2064 (2008).
[16] J. Ghose, J. Solid State Chem. **79**, 189 (1989).
[17] B. T. Liou *et al.*, Appl. Phys. A **81**, 651 (2005).
[18] Y. Nambu *et al.*, Phys. Rev. B **79**, 214108 (2009).